Journal of Materials Chemistry B

Accepted Manuscript

ROYAL SOCIETY OF CHEMISTRY

www.rsc.org/materialsB

Journal of
Materials Chemistry B

Cite this: DOI: 10.1039/c0xx00000x

www.rsc.org/xxxxxx

PAPER

A novel self-assembled targeted nanoparticle platform based on carboxymethylcellulose co-delivery of anticancer drugs

Lin Dai,[a] Ke-Feng Liu,[a] Chuan-Ling Si,[b] Jing He,[a] Jian-Du Lei,*[a] and Li-Qun Guo[c]

Received (in XXX, XXX) Xth XXXXXXXXX 20XX, Accepted Xth XXXXXXXXX 20XX
DOI: 10.1039/b000000x

Single-drug therapy for cancer is greatly hampered by its non-specific delivery to the target tissue, limited efficacies, poor tolerability, and resistance profiles. In order to overcome this limitation, we developed a new targeted nanoparticle platform for co-delivery of the two different anticancer drugs. A conjugate based on carboxymethylcellulose (CMC) was first synthesized by introducing hydrophilic molecules (PEG), target molecules (folate), and drug molecules (betulinic acid) to CMC. Then another anticancer drug hydroxycamptothecine (HCPT) was encapsulated into the nanoparticles from the conjugate using a simple nanoprecipitation method. The obtained nanoparticles possessed appropriate size (~180 nm), high drug loading efficiency (~23 wt% BA, 21.15wt% HCPT), slowly drug release rate, higher blood circulation half-time of free BA (6.4-fold) and HCPT (6.0-fold), and high synergetic activity of BA and HCPT toward cancer cells. Furthermore, the targeted nanoparticles showed rapid cellular uptake by tumor cells. The antitumor effect of the nanoparticles in a mouse tumor xenograft model exhibited much better tumor inhibition efficacy and fewer side effects than that of BA and HCPT, strongly supporting their application as efficient carriers for anticancer therapy.

1. Introduction

Many anticancer drugs were discovered in a National Cancer Institute drug screening program of natural plant extracts, such as hydroxycamptothecine (HCPT) and betulinic acid (BA).[1, 2] They were often required a high drug dose to kill the whole cancer cell population; whereas they always show limited efficacies, poor tolerability, and resistance profiles. Therefore, cancer chemotherapy routinely involves administration of different therapeutic agents.[3] The main advantage of combination therapy over monotherapy is the ability to hit different disease targets simultaneously, which results in increased activity and reduced toxicity.[4] Both HCPT and BA are potent Topoisomerase (Top) inhibitors, but HCPT just interferes with the action of Top I. Certain clinical limitations such as resistance of cancer cells impair its clinical application.[5] It has been proven that the increase of Top II activity occurs in cancer cells resistant to HCPT.[6] BA has been reported to be a catalytic inhibitor of TOP I and II activity. Top II inhibitor shows a collateral cytotoxicity on the HCPT adapted cancer cells. Therefore, the concomitant use of both Top I and Top II inhibitors might elicit synergistic effects and prevent the emergence of drug resistance. In addition, clinical application of poorly soluble drugs, such as BA and HCPT, in cancer therapy is limited. This is likely due to the very lipophilic characteristics and its consequently poor solubility, relatively short half-life, and low bioavailability,[1, 7] which makes *in vivo* application difficult. This is often a hampering step during drug development, so developing a convenient and safe delivery system to maximize the therapeutic efficacy at tumor sites while minimizing the side effects is therefore a challenging endeavor. Currently, a variety of drug delivery systems such as liposomes, dendrimers, microcapsules, and nanoparticulate drug carrier have been developed to address these problems and further to promote sustained, controlled, and targeted delivery of poorly watersoluble anticancer drugs.[8] Of all these delivery systems, nanoparticulate drug carrier, in which excipient, emulsion, or nanocrystalline methods are typically applied to enhance the bioavailability of insoluble therapeutics.[9, 10]

Polymeric amphiphiles consisting of hydrophilic and hydrophobic segments have received increasing attention because they can form self-assembled nanoparticles and exhibit unique physicochemical characteristics such as a nanoparticle structure and thermodynamic stability.[11, 12] Generally, the hydrophobic blocks of the copolymer can segregate into the core of the nanoparticle in an aqueous environment, whereas the hydrophilic blocks form the corona or outer shell. The inner core can serve as a nano-container for hydrophobic anticancer drugs. Such core-shell architecture of the polymeric nanoparticles is essential for their utility as novel functional materials for drug delivery. Moreover, compared with other delivery systems, nanoparticles show advantages in passive tumor targeting through the leaky vasculature via the enhanced permeability and retention (EPR) effect due to their small size ranging from 10 to 200 nm, which is small enough to avoid filtration by the lung and spleen. Therefore,

Journal of
Materials Chemistry B

Cite this: DOI: 10.1039/c0xx00000x

www.rsc.org/xxxxxx

PAPER

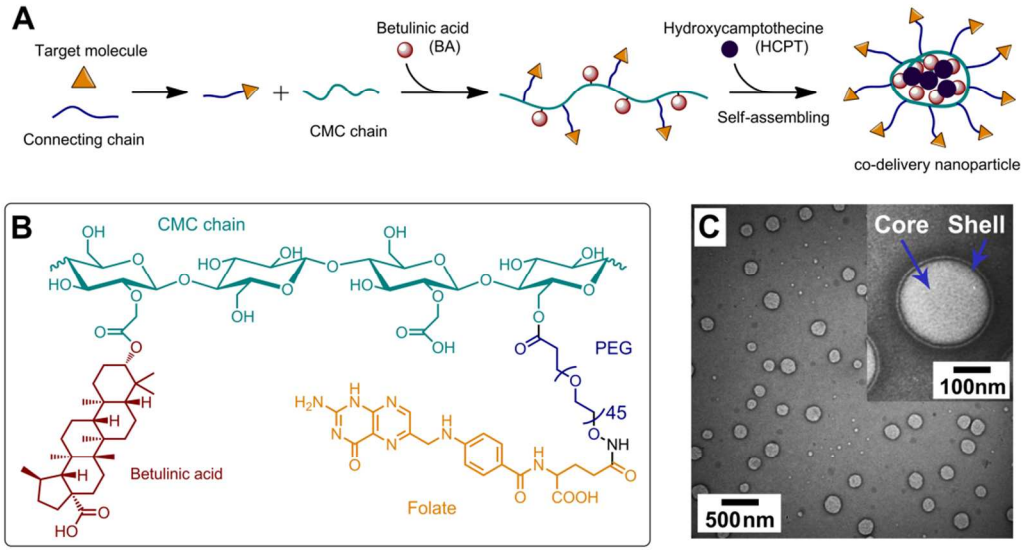

Fig. 1 Schematic design of the conjugate synthesis and nanoparticle preparation. (A) The conjugate was synthesized by introducing target molecules (folate), connecting chain (PEG), and drug molecules (BA) to carboxymethylcellulose (CMC), and then self-assembled into nanoparticle with free HCPT encapsulated. (B) The chemical structure of the conjugate. (C) TEM images of FPCB/HCPT NPs. Inset: single nanoparticle TEM image at higher resolution.

drug delivery using polymeric nanoparticles is an effective strategy for passive tumor targeting.[13-15] Developing a biocompatible polymer backbone with a good safety profile for drug delivery remains challenging. Water-soluble polysaccharides, in particular cellulose derivatives, are emerging as novel carriers of drugs because of their solubility and known safety profiles *in vivo*. Certain classes of polysaccharides are approved as excipients for oral, transcutaneous, and parenteral drug administration (FDA inactive ingredients database),[16] but when referenced against the synthetic polymer field, little work has been done with these biocompatible polysaccharides in the contemporary nanoparticle drug delivery field.[17-19] Auzenne et al. conjugated paclitaxel to hyaluronic acid, and performed *in vitro* and *in vivo* efficacy assays.[20] Mice were implanted with ovarian carcinoma xenografts in the peritoneal cavity, and were treated with an intraperitoneal injection of 200 mg/kg paclitaxel-hyaluronic acid, a treatment which effectively cured the mice and was well tolerated. Ernsting et al using carboxymethylcellulose (CMC) as a polymer backbone for the delivery of docetaxel. *In vitro*, the cytotoxicity of the optimal conjugate formulation was improved by 2−40-fold compared to free docetaxel.[21]

However, a more effective and active targeting system has been further needed to enhance intracellular uptake of drug within cancerous cells at the tumor site.[22, 23] Among the various targeting moieties and ligands, the folate receptor (FR) is a high-affinity, membrane-anchored protein which mediates the transport of folic acid and its conjugates into the cell interior by endocytosis.[24, 25] FR is overexpressed in many human cancer cells, including malignancies of the ovary, brain, kidney, breast, and lung.[26-30] Therefore, folate has been identified as a targeting moiety to facilitate the targeted delivery of anticancer drugs. Herein, we design a delivery system for insoluble anticancer drug BA by CMC nanoparticles. The amphiphilic property of the prepared CMC conjugate is investigated owing to the introduction of BA, folate (F), and polyethylene glycol (PEG) to CMC backbones. Moreover, a cell-specific targeting F-PEG-CMC-BA nanocarrier to deliver another anticancer drug is developed, where in the hydrophobic anticancer drugs HCPT are entrapped into F-PEG-CMC-BA conjugate. Finally, the *in vitro* and in *vivo* antitumor activity of F-PEG-CMC-BA/HCPT nanoparticles was investigated.

2. Experimental Details

2.1. Reagents and Materials

Sodium carboxymethylcellulose (CMC-Na) (CEKOL 30000, MW = 275K, degree of substitution (DS) = 0.82) was purchased from Sigma-Aldrich, and is an FDA and EU foodgrade material. Acetic anhydride, sulfuric acid, acetone, acetonitrile, pyridine (Py), methoxy poly(ethylene glycol) carboxyl (M-PEG-CO0H, M_W = 2000), amine polyethylene glycol carboxyl (NH_2-PEG-CO0H, M_W = 2000), 1-ethyl-3-(3-dimethylaminopropyl)-carbodiimide HCl (EDC HCl), *N*-hydroxysuccinimide (NHS), 4-dimethylaminopyridine (DMAP), and diethyl ether were purchased from Sigma Aldrich. BA was purchased from Chengdu Preferred Biotechnology Co., Ltd. (Chengdu, Sichuan, China).

Vivaspin MWCO 10 kDa, 3.5 kDa and 2 kDa ultracentrifugation filters were purchased from Fisher (Ottawa, ON, Canada). All other reagents were purchased from Sigma Aldrich.

Penicillin and streptomycin, Gibco Dulbecco's Phosphate-Buffered Saline (DPBS), and Gibco Dulbecco's Modified Eagle's Medium (DMEM) were all bought from Invitrogen. Fetal bovine serum (FBS) was from HyClone. Cell-Counting Kit-8 (CCK-8) was supplied by the Dojindo Laboratories. Human lung cancer cells (A549) and murine Lewis lung carcinoma (LLC) cells were obtained from the Peking University Health Science Center (Beijing, China) and were cultured in the listed medium: A549 by RPMI 1640 with 10% FBS, 1% streptomycin–penicillin and LLC by DMEM with 10% FBS, 1% streptomycin–penicillin. All cell lines were maintained in an incubator supplied with a 5% CO_2/95% air humidified atmosphere at 37 °C.

2.2. Animals and Ethics

Female C57BL/6 mice, 6-7 weeks age, were purchased from Beijing HFK BIOSCIECE CO., LTD. All the animal experiments were consistent with the guidelines set by the National Institutes of Health (NIH Publication No. 85-23, revised 1985) and were approved by the Experimental Animal Ethics Committee, Beijing.

2.3. Synthesis of Polyethylene glycol-Folate (PEG-F)

Conjugation of folic acid to PEG was adapted from Wang at al. [31] (Fig. 2A). Folic acid (440 mg, 1.0 mmol) dissolved in 20 mL DMSO was reacted with EDC (383 mg, 2.0 mmol) and NHS (230 mg, 2.0 mmol) at 50 °C for 6 h. It is generally known that folate has two α- (high affinity for the FR) and γ-carboxylic acids, but the γ-carboxylic acid is more selectively activated due to its higher reactivity.[32, 33] The resulting folate-NHS was reacted with ethylenediamine (781 mg, 13.0 mmol) and pyridine (500 mg, 6.3 mmol) at room temperature overnight. The folylethylamine (folate-NH_2) was precipitated by the addition of excess acetonitrile, and the precipitate was filtered and washed with diethyl ether before drying under vacuum to get yellow powder. This was added to the NH_2-PEG-COOH 2000 (1.60 g, 0.8 mmol), dissolved in 20 mL of MeCN, and activated by EDC (0.38 g, 2.0 mmol), NHS (0.23 g, 2.0 mmol) and DMAP (0.024 mg, 0.2 mmol) for 8 h. The unreacted folate-NH_2 was removed by dialysis (MWCO 2 kDa).The prepared PEG-F was lyophilized as a yellow powder (1.43 g).

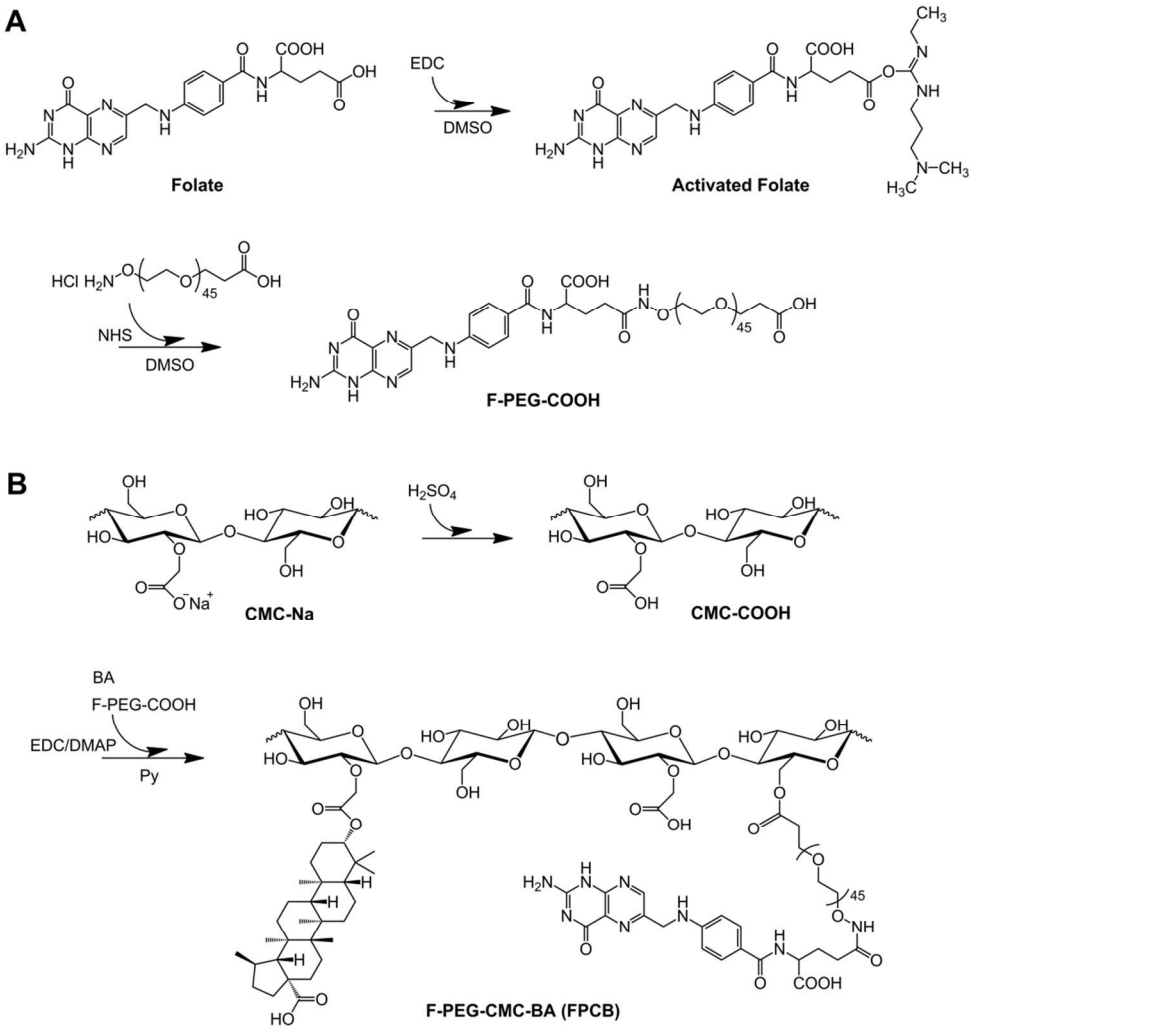

Fig. 2 (A) Synthesis folate-PEG-COOH conjugate (F-PEG-COOH). (B) Synthesis folate-PEG-carboxymethylcellulose-betulinic acid conjugate (F-PEG-CMC-BA, FPCB). Note that the distribution of BA or F-PEG-COOH substitutions is random: for ease of depiction, monomers are drawn in simplified form.

Journal of Materials Chemistry B

Cite this: DOI: 10.1039/c0xx00000x

www.rsc.org/xxxxxx

PAPER

2.4. Synthesis of F-PEG-CMC-BA (FPCB) Copolymer

CMC-Na (0.20 g) was weighed into a round-bottom flask, and was suspended in 20% sulfuric acid (5 mL) with vigorous stirring at room temperature for 2 h. The slurry of CMC-COOH was washed with water until the water tested neutral, and then washed with 3 × 30 mL glacial acetic acid volumes. The CMC-COOH was transferred to a round-bottom flask and dissolved in 20 mL of dry Py and maintained by gentle heating. BA (0.47 g, 1.00 mmol), PEG-F (0.04 g, 0.16 mmol), EDC (0.46 g, 2.40 mmol), NHS (0.28 g, 2.40 mmol), and DMAP (0.03 g, 0.24 mmol) were successively added to the mixture, and the reaction was allowed to proceed at 35 °C (Fig. 2B). After overnight stirring, deionized water was gradually added and the solution was dialyzed against deionized water for 48 h in a dialysis membrane (MWCO 3.5 kDa). After lyophilization, FPCB conjugate was obtained as a light yellow powder. ^{1}H-NMR analysis ($CDCl_3$) was conducted to confirm the presence of BA, PEG, and folate. The folate content was determined by UV measurement.

2.5. Synthesis of PEG-CMC-BA (PCB) Copolymer

CMC-COOH (0.20 g) was dissolved in 20 mL of dry Py and maintained by gentle heating. BA (0.47 g, 1.00 mmol), M-PEG-COOH (0.03 g, 0.16 mmol), EDC (0.46 g, 2.40 mmol), NHS (0.28 g, 2.40 mmol), and DMAP (0.03 g, 0.24 mmol) were successively added to the mixture, and the reaction was allowed to proceed at 35 °C. After overnight stirring, deionized water was gradually added and the solution was dialyzed against deionized water for 48 h in a dialysis membrane (MWCO 3.5 kDa). After lyophilization, PCB conjugate was obtained as a white powder.

2.6. Preparation of F-PEG-CMC-BA/HCPT Nanoparticles (FPCB/HCPT NPs)

Nanoparticles were prepared by a nanoprecipitation method as described previously.[21] FPCB conjugate (0.20 g) and HCPT (0.10 g) in 0.2 mL of dry DMSO was mixed and added dropwise to a vortexing solution of 3.8 mL phosphate buffered saline (PBS) solution (pH 7.4) in a 15 mL conical tube. Vortexing was maintained for 1 min after solution addition. The resulting FPCB/HCPT NPs solutions were transferred to a MWCO 10 kDa cartridge, and dialyzed against PBS solution (pH 7.4, 100 mL) for 6 h with two exchanges of dialysate, and spun at 3000 rpm to concentrate the particles. The size of the particles was determined by dynamic light scattering with a particle analyzer (Zetasizer Nano-ZS, Malvern Instruments Ltd., Malvern, UK). FPCB NPs and PCB NPs were similarly prepared to that for FPCB/HCPT NPs.

2.7. TEM Analysis

PCB NPs, FPCB NPs, and FPCB/HCPT NPs were diluted 100× in deionized water, and a 2 μL aliquot of solution was pipetted onto the surface of Formvar coated copper TEM grids (TedPella, Redding, CA) and allowed to air-dry. Analysis was performed on a JEM-100CXa TEM at an acceleration voltage of 100 kV.

2.8. Determination of Drug Loding and *in vitro* Drug Release

A mass or molar drug/carrier ratio for the conjugate were determined as described here. BA was detected by UV-Vis spectrophotometer as reported earlier.[34] Briefly, BA and folate were dissolved in 80% (wt) of acetonitrile water solution and water respectively. Then the UV absorbance of the derivative of BA and folate was determined at 210 nm and 280 nm respectively, for five different concentrations.

The releases of BA and HCPT from the FPCB/HCPT NPs were analyzed by a dialysis method. FPCB/HCPT NPs PBS solution (1mg/mL, 5 mL) at pH 7.4 was loaded into a dialysis bag (MWCO 3.5 kDa). The dialysis bag was then immersed in 200 mL of PBS buffer (pH 7.4) at 37 °C with gentle agitation. PBS medium (2 mL) was withdrawn at timed intervals and the BA and HCPT concentration in the medium was determined by HPLC method (BA: 210 nm, 85:15 mixture (v/v) of acetonitrile-water as a mobile phase, flow rate at 1.0 mL/min; HCPT: 254 nm, 30:70 mixture (v/v) of acetonitrile-water as a mobile phase, flow rate at 1.0 mL/min) using a reverse phase column (C18). The amount released was then calculated. Each stability profile represents the average of three independent runs with the same sampling schedules. The standard deviation of each point is typically 2% or less. Drug loading efficiency (DLE) were calculated according to the following equation: DLE (%) = (weight of loaded drug/weight of nanoparticles) × 100%. Esterase (30 units) was added into the dialysis bag when the BA and HCPT release in the presence of esterase was studied.

2.9. Hemolysis Assay

The hemolytic activity of polymer solutions was investigated as reported earlier.[35, 36] Briefly, fresh blood samples were collected through cardiac puncture from rats. 10 mL of blood was added with EDTA-Na_2 immediately to prevent coagulation. The red blood cells (RBCs) were collected by centrifugation at 1500 rpm for 10 min at 4 °C. After washing in ice-cold DPBS until the supernatant was clear, erythrocytes were diluted at a final concentration of 5×10^8 cells/mL in ice-cold DPBS. 1 mL FPCB NPs or FPCB/HCPT NPs or PEI_{25K} solution (1 mg/mL and 0.1 mg/mL) was mixed with 1 mL erythrocyte suspension. DPBS and 1% Triton X-100 in DPBS were used as negative control (0% lysis) and positive control (100% lysis), respectively. Samples were incubated for 1 h at 37 °C under constant shaking. After centrifugation at 1500 rpm for 10 min at 4 °C, supernatant was analyzed for hemoglobin release at 541 nm using an infinite M200 microplate spectrophotometer (Tecan, Switzerland). Hemoglobin release was calculated as $(OD_{sample}–OD_{negative\ control})/(OD_{positivecontro}–OD_{negative\ control}) \times 100\%$. Hemolysis was

determined from three independent experiments.

2.10. *In vitro* Cell Cytotoxicity

CCK-8 assay was used for cell viability evaluation of different samples. Briefly, two types of lung cancer cells LLC and A549 cells were respectively seeded at a density of 3×10^3 and 4×10^3 cells/well in 180 μL culture medium within a 96-well plate (Corning, USA) and incubated overnight. Then, the cells were treated with various samples (BA, HCPT, PCB NPs, FPCB NPs, and FPCB/HCPT NPs) at 37 °C in a humidified incubator with 5% CO_2 for 72 h, where the samples of the BA were dissolved in dimethylsulfoxide (Merck, Darmstadt, Germany) and diluted into tissue culture medium before assay. BA dose ranged from 0.3 to 60 μg/mL, PCB NPs, FPCB NPs, and FPCB/HCPT NPs dose equal to BA. HCPT dose equal to the HCPT content in FPCB/HCPT NPs. 20 μL of CCK-8 solution was added to each well of the plate and incubated for another 1 h at 37 °C. The absorbance at 450 nm was measured an infinite M200 microplate spectrophotometer. Percent viability was normalized to cell viability in the absence of the samples. The IC_{50} was calculated as polymer concentrations which inhibited growth of 50% of cells relative to non-treated cells according to Unger et al. [37] IC_{50} was calculated using the Boltzmann sigmoidal function from Origin® 8.6 (OriginLab, Northampton, USA). Data are representative of three independent experiments.

We evaluate the synergistic effects between BA and HCPT in the FPCB/HCPT NPs by applying the combination index (CI) = $BA_{Combined}/BA_{Single}$ + $HCPT_{Combined}/HCPT_{Single}$, whereby $BA_{Combined}$ and $HCPT_{Combined}$ represents the IC_{50} of drugs used in the combination treatment, and BA_{Single} and $HCPT_{Single}$ represents single drug IC_{50}. An index lesser than 1 denotes drug synergism while larger than 1 is an antagonistic effect.[38]

2.11. Cellular Uptake Study

Cellular uptake and distribution of HCPT from developed nanoparticles were observed by confocal laser scanning microscopy (CLSM, TCS SP5, Leica). After LLC cells achieved 70-80% confluency, the cells were trypsinized and seeded onto culture slides (BD Falcon, Bedford, MA) at a density of 6.0×10^5 cells per well (surface area of 8 cm^2 per well) and incubated for 24 h at 37 °C. HCPT (IC_{50}), alone or entrapped in nanoparticles, was added and incubated for 4 h at 37 °C. After incubation, all reagents were removed. Cells were washed with PBS (pH 7.4) at least 3 times and fixed with 4% formaldehyde solution for 10 min. The liquid content was then dried completely. DMEM medium with 4',6-diamidino-2-phenylindole (DAPI) (H-1200; Vector Laboratories, Inc., Burlingame, CA) was added to prevent fading and to stain nuclei. Nanoparticles were detected using HCPT autofluorescence at 488 nm.

2.12. Pharmacokinetic Experiments in Mice

24 tumor-free healthy C57BL/6 female mice were divided into four groups at random. Group 1 and 2 was treated with free BA and free HCPT injection, respectively, groups 3 and 4 with PCB NPs and FPCB/HCPT NPs, respectively, via the tail vein. After intravenous administration, blood samples were collected at 0.083, 0.25, 0.5, 1, 2, 5, 10, 24, 48, 72 h from the orbital plexus and centrifuged immediately at 3000 rpm for 10 min at 4 °C. The plasma was frozen at -20 °C until assay. To determine the level of total BA or HCPT in each plasma sample, 100 μL of plasma was mixed with 50 μL of 0.1 N NaOH for 15 min in water bath at 37 °C, allowing the hydrolysis of the nanoparticles. After that, 0.1 N HCl (50 μL) was added, followed by 100 μL methanol. After vortexed for 2 min, the mixture was sonicated for 5 min and centrifuged at 5000 rpm for 5 min. The clear supernatant was dried under nitrogen, reconstituted by 100 μL methanol before HPLC analysis.[39] The HPLC employs a VYDAC 214TP54 (C18, 5μm, 4.6 × 250 mm) with a UV detector, using a gradient of 60% of acetonitrile in 0.05% TFA at a flow rate of 1 mL/min. Blood circulation data were plotted as the blood BA or HCPT levels with the unit of percentage of injected dose per gram (% ID/g) against time after injection.

2.13. *In vivo* Efficacy Studies

Subcutaneous tumor xenograft models were established in the right axillary flank region of C57BL/6 female mice (6-7 weeks) by injecting 1×10^6 LLC cells in 200 μL DMEM medium per mouse. Treatments were initiated when tumors reached an average volume of 100 to 150 mm^3, and this day was designated as day 0. On day 0, these mice were randomly divided into six groups (n = 6) and administered intravenous injection with PBS (control), free BA (10 mg/kg), free HCPT (10 mg/kg), PCB NPs, FPCB NPs, and FPCB/BA NPs (equal to 10 mg/kg BA), respectively, on days 0, 2, 4, 6, and 8. In the observation phase, mice were monitored for tumor sizes and body weights every other day. Tumor volume was calculated using the formula: Tumor volume (TV) = $(L \times W^2)/2$, where L is the longest and W is the shortest tumor diameter (millimeter). Relative tumor volume (RTV) was calculated at each measurement time point (where RTV was equal to the tumor volume at a given time point divided by the tumor volume prior to initial treatment). For efficacy studies, the percentage of tumor growth inhibition (%TGI) was calculated using the following formula: %TGI = $[(C - T)/C] \times 100\%$, where C is the mean tumor volume of the control group at a specified time and T is the mean tumor volume of the treatment group at the same time. To monitor potential toxicity, we measured the weight of each mouse. For humane reasons, animals were killed and regarded as dead if the implanted tumor volume reached to 5000 mm^3 or at the end of the experiment (> 6 weeks). To further evaluate the hematological toxicity of different nanoparticles, we collected 200 μL of blood of each mouse after final administration to test the white blood cell number (WBC) using a hematology analyzer (MEK-7222K, Nihon Kohden Celltac E).

2.14. Detection of Allergic Reaction

Toxic side-effects of the current chemotherapeutical drugs are often causing a severe reduction in the quality of life, so the detection of allergic reaction is very necessary and important. Six groups of tumor bearing mice (26-28 g, n = 6) were used in allergy testing studies in five samples (control, BA, HCPT, PCB NPs, FPCB NPs, and FPCB/HCPT NPs). The five samples were administrated via tail intravenous injection every two days (BA: 10 mg/kg; HCPT: 5 mg/kg; PCB NPs, FPCB NPs, and FPCB/BA NPs were equal to 10 mg/kg BA). After administration with different samples for 10 days, orbit blood of mice in different groups was collected and centrifuged. Serum samples were analyzed according to the procedure of Mouse IgE ELISA.

2.15. Statistical Analysis

All experiments in this study were performed at least three times, and the data were expressed as the means standard deviation (SD). Statistical analyses were performed by analysis of variance (ANOVA). In all analyses, $p < 0.05$ was taken to indicate statistical significance.

3. Results and Discussion

Although many works has been reported cellulose nanoparticle delivery system could be accumulated to the solid tumor site in a passive targeting manner by an EPR effect,[21, 40, 41] cell-specific targeting ability of cellulose-based nanoparticle delivery system is highly desirable. The main goal of this work was to prepare a cellulose-based nanoparticle delivery system to leverage the EPR effect and protect the drug from early release or alteration, to incorporate folate to target tumor cells, and to release two different anticancer drugs (BA and HCPT) in a controlled and slow release mechanism in the target tissue. CMC was selected based on its known safety profile as an excipient, and due to the reasonable stability of the backbone in human physiological conditions, ensuring maintenance of macromolecule integrity during circulation. Herein, to increase the hydrophilic ability and chain length, the NH_2-PEG-COOH was selected to conjugate with folate. After an acylation reaction, the resulting polyethylene glycol-folate contained a free carboxyl group at the distal end of PEG for subsequent use in a CMC conjugate. Due to the necessary chemical functionalization of CMC, the PEG-F conjugate displayed an amphiphilic property capable of physically entrapping with hydrophobic anticancer drug BA, thereby forming FPCB NPs. The incorporation of folate at the distal end was expected to improve the specificity toward cancer cells overexpressing a folate receptor as well as enhance the cellular uptake of FPCB NPs. The designed strategy of nanoparticle delivery system is shown in Fig. 1 and 2.

3.1. Preparation of FPCB Copolymer

Direct proofs confirming BA, PEG, and folate conjugated onto CMC came from Fig. 3. Partial structure of BA can be identified at peaks from 0.8 to 1.4 ppm,[42] the broad peaks of PEG from 3.6

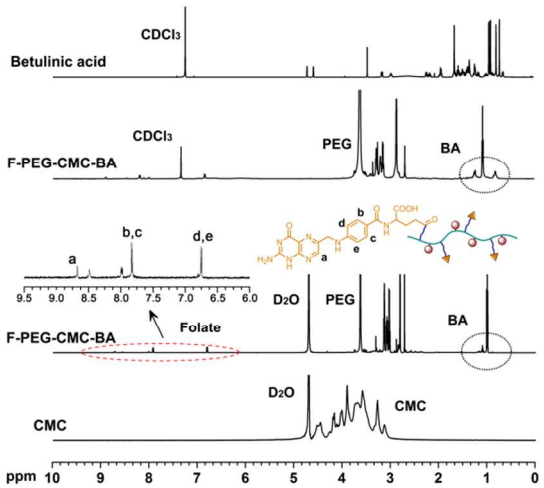

Fig. 3 ^{1}H-NMR spectra of BA in $CDCl_3$, FPCB in $CDCl_3$, FPCB in D_2O, and CMC in D_2O.

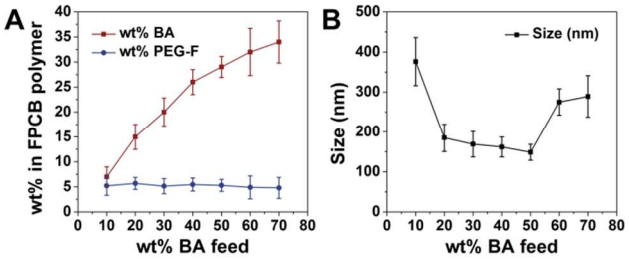

Fig. 4 Optimization of FPCB NPs formulation. (A) BA was fed into the reactions at different ratios, and PEG was maintained at a feed of ~5 wt%. The resulting conjugates were characterized for mass fraction of BA and PEG. (B) FPCB conjugates formed nanoparticles when they contained a defined range of BA content. Conjugates with compositions outside this range formed larger less defined particles, or precipitated.

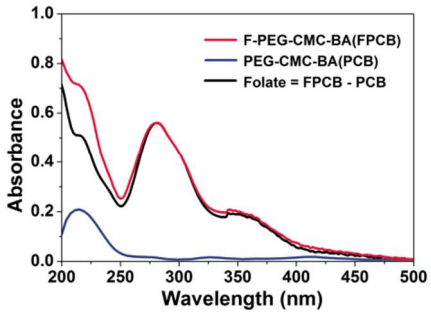

Fig. 5 Quantitative analysis of folate and BA content as determined by UV method.

to 3.7 ppm in the presence of $CDCl_3$.[43] Interestingly, and the proton peaks of folate at 8.63 (s, C7-H of folate, 1H), 7.81 (d, 2'6' H of folate, 2H), 6.75 (d, 3'5' H of folate, 2H) taken in D_2O as a solvent was similar to the $CDCl_3$.[31] The final FPCB was a light yellow powder, readily soluble in acetonitrile and chloroform. See Fig. 3 for the ^{1}H-NMR spectra of CMC, BA, and the final FPCB conjugate. By ^{1}H-NMR analysis, the peak assignments were identical in all polymer products, varying only in the integration of peaks assigned to PEG, folate, and BA.

Conjugates were prepared with a range of BA wt% feeds (10, 20, 30, 40, 50, 60, 70 wt%). As shown in Fig. 4A, all the conjugates exhibited a similar wt% for PEG-F (4.8 to 5.2 wt%) and the wt% for BA increased with increasing feeds. Conjugates prepared across the 10-70 wt% feed range of composition were tested for particle forming size: as seen in Fig. 4B, conjugates prepared with 20-50 wt% BA feed yielded particles ranging 148-185 nm. For the preferred composition (50 wt% BA feed), the FPCB conjugate contained 29.02 ± 2.10 wt% BA and 5.29 ± 1.22 wt% PEG-F. For effective nanoparticle forming properties, the hydrophobic BA and hydrophilic PEG-F elements of the FPCB macromolecule were balanced, so that when these amphiphilic structures contacted isotonic aqueous solution, they would assemble into stable nanoparticles and protect the drug cargo from direct exposure to serum enzymes.[44] HCPT, a potent hydrophobic anticancer agent, was readily loaded into FPCB NPs.

Fig. 5 presents the UV spectra of FPCB, PCB, and folate (FPCB - PCB). Obviously, the characterized peak of folate for FPCB and folate appeared at 210 and 360 nm. For the similar mol % BA of FPCB and PCB, the folate content in FPCB was calculated by equation $ABS_F = ABS_{FPCB} - ABS_{PCB}$, assuming that the FPCB and PCB in acetonitrile has the same molar extinction

Journal of Materials Chemistry B

Dynamic Article Links ►

Cite this: DOI: 10.1039/c0xx00000x

PAPER

www.rsc.org/xxxxxx

Table 1 Particle Size and Drug Loading Efficiency of Nanoparticles

Compound	size (nm)	PEG-F (wt%)	DLE of BA (wt %)	DLE of HCPT (wt %)
PCB NPs	135.65 ± 7.28	---	29.46 ± 2.35	---
FPCB NPs	148.89 ± 6.73	5.29 ± 1.22	29.02 ± 2.10	---
FPCB/HCPT NPs	186.23 ± 10.52	4.17 ± 0.89	22.88 ± 2.05	21.15 ± 2.43

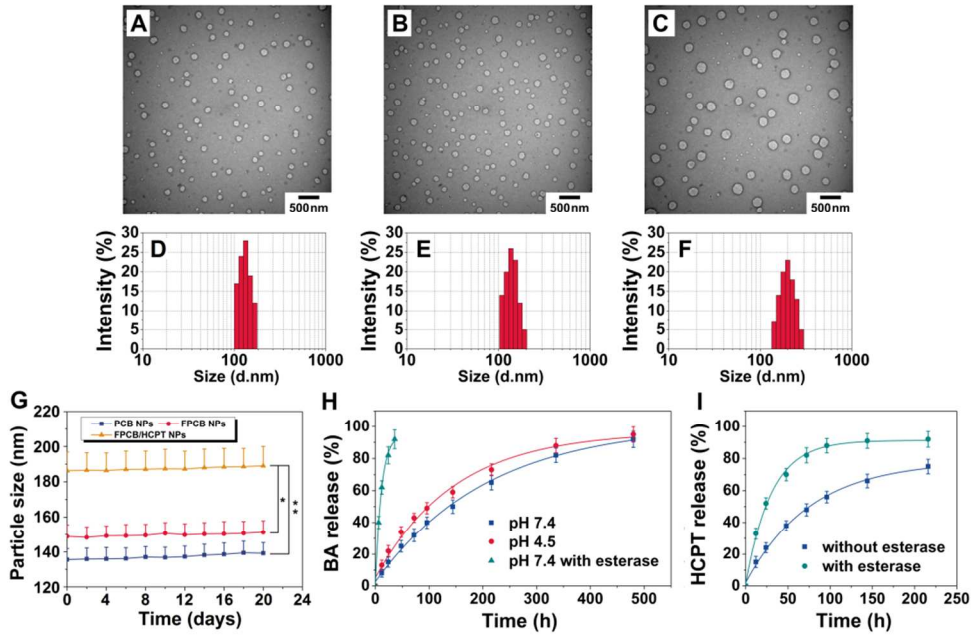

Fig. 6 TEM images and particle size distribution of PCB NPs (A, D), FPCB NPs (B, E), and FPCB/HCPT NPs (C, F) loading with 22.88 ± 2.05 wt% BA, 21.15 ± 2.43 wt% HCPT. Scale bars were 500 nm. The size distribution of the nanoparticles for 20 days storage at 4 °C (*p < 0.05, **p < 0.01, n = 3) (G). BA release kinetics (H) and the HCPT release kinetics in PBS at pH 7.4 and 37 °C from the FPCB/HCPT NPs (I).

coefficients and that both followed Lambert-Beer's law (Table 1).[31]

3.2. Nanoparticle Formulation

Nanoparticles were prepared using the well-established nanoprecipitation method [45] by slow addition of a DMSO solution of PCB or FPCB into aqueous media (10× dilution), and desired particles were produced provided the concentration of FPCB in the organic solvent solution ranged from 20 to 100 mg/mL. It was observed that particles formed from 50 mg/mL solutions were approximately 150 nm in size (Table 1, Fig. 6A and B), and particles formed from 20 mg/mL solutions were smaller (90-110 nm).

We have encapsulated HCPT as a model chemotherapy drug into the FPCB NPs. HCPT is a kind of hydrophobic drug which can be loaded into the hydrophobic core of the nanoparticles due to the BA hydrophobic core, whereas the hydrophilic part came from the water-soluble blocks of cellulose and PEG immersed in the water to formulate the outer shell of composite core-shell nanoparticles.[46] As determined by transmission electron microscopy (TEM) and dynamic light scattering (DLS), the results showed that the drug-loaded nanoparticles (FPCB/HCPT NPs) exhibited bigger spherical shape than the blank ones and FPCB NPs was a little bigger than PCB NPs (Fig. 6A-F). The increase of the nanoparticle sizes after loaded with HCPT might be due to the insertion of the hydrophobic drug into the nanoparticle. The exact cause is still under investigation.[47]

The critical aggregation concentration (CAC), determined by the DPH assay, was 0.8 μg/mL, which is similar to most reported nanoparticles delivery systems. As FPCB NPs was stable at the CAC, it is probable that these particles will remain stable at high dilution in biological systems. For example, in a 27 g mouse model treated at 10 mg/kg BA, 200 μL of FPCB/HCPT NPs administered intravenous injection (5.9 mg/mL FPCB/HCPT NPs) would be diluted in ~2 mL blood volume to 0.59 mg/mL FPCB/HCPT NPs. Considering the scenario when 90% of particles are out of circulation, the concentration of FPCB/HCPT NPs would be still well above CAC.

As shown in Fig. 6G, the average particle size of the nanoparticles (redispersion in PBS) hardly changed during the investigation period, i.e. the PCB NPs, FPCB NPs, and FPCB/HCPT NPs exhibited a good redispersion stability.

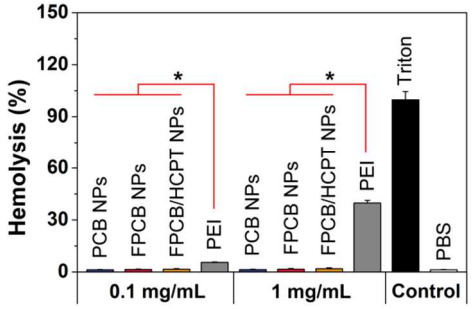

Fig. 7 *In vitro* hemolysis assay of PCB NPs, FPCB NPs, and FPCB/HCPT NPs compared to PEI_{25K} and Triton X-100 measured at 541 nm. Values are reported as the mean ± SD for triplicate samples.

3.3. *In vitro* Drug Release

Nanoparticles were first placed in aqueous solutions that simulated biological fluids, and *in vitro* BA and HCPT release kinetic were quantified by HPLC analysis. FPCB/HCPT NPs very slowly hydrolyzed and released the BA at a weakly acidic or neutral pH without the common burst release phenomenon found in drug-loaded nanoparticles (Fig. 6H). However, in the presence of esterase, which is abundant in cytoplasm, FPCB/HCPT NPs quickly hydrolyzed and released the BA. Therefore, FPCB/HCPT NPs was a prodrug for intracellular release of BA. The resulting release data appear in Fig. 6I. The amount of BA or HCPT loading as listed in Table 1.

The utility of the FPCB NPs as carriers for other drugs was also demonstrated by the controlled release of HCPT (Fig. 6I). The FPCB/HCPT NPs released HCPT in a controlled manner, suggesting that the HCPT had to slowly diffuse out through the nanocapsule membrane. Adding esterase promoted HCPT release due to the hydrolysis of FPCB.[47]

3.4. Hemolysis Study

Detrimental interaction of conjugates with blood constituents such as RBCs must be avoided when these conjugates are injected into the blood circulation as a carrier for drug delivery.[36] Erythrocytes were incubated with two concentrations of polymer as 1 mg/mL and 0.1 mg/mL, for 1 h at 37 °C. Hemolysis was evaluated by measuring the amount of hemoglobin released in the supernatant at 541 nm (Fig. 7). Triton X-100 was used as positive control, which induced full hemoglobin release. All of samples at concentrations of 1 mg/mL and 0.1 mg/mL showed a comparable hemoglobin release to blank values (<5%), which was significantly lower than similar concentrations of PEI_{25K}, a cationic polymer known to have significant hemolytic effect. Despite BA and HCPT was cytotoxic to the RBCs,[48] these nanoparticles released a little BA or HCPT during the short incubation period (approximately 1 h), suggesting the excellent safety of all the nanoparticles.

3.5. *In vitro* Cytotoxicity

To ensure the effective of the nanoparticles before their entry into human application, *in vitro* cytotoxicity should be considered upfront.[49, 50] To examine the cytotoxicity of BA, HCPT, and the nanoparticles, a CCK-8 assay was conducted after incubating cells treated with different formulations. The response of LLC and A549 cells was tested *in vitro* by seeding the cells and exposing them to various concentrations of PCB NPs, FPCB NPs, FPCB/HCPT NPs, CMC-PEG, free BA, or free HCPT. Cells were exposed to drug for 24, 48 or 72 h. Analysis of *in vitro* cytotoxicity measurements showed that BA (10 μg/mL) and HCPT (10 μg/mL) induced cell death which was dependent upon length of incubation. As shown in Fig. 8A and B, the time-dependent cytotoxic effect of the FPCB/HCPT NPs was evident, which indicated that 30.6% LLC and 32.8% A549 survival after 24 h, 18.6% LLC and 20.5% A549 survival after 48 h, 10.0% LLC and 9.1% A549 survival after 72 h at 10 μg/mL (equivalent to native BA). The drug release from the FPCB/HCPT NPs when incubated with cells is possibly from the diffusion of drug molecules in the nanoparticles and the degradation of nanoparticles, which is the main mechanism of drug release observed for polymer nanoparticles.[51]

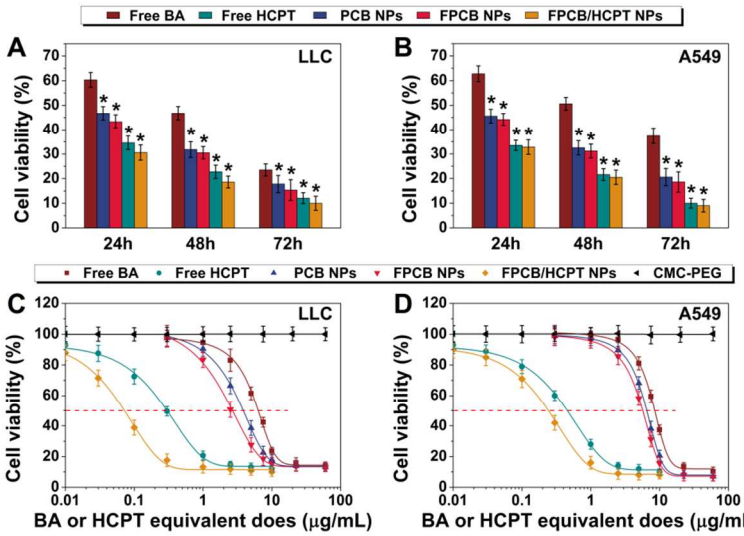

Fig. 8 Cellular cytotoxicity of BA, HCPT, PCB NPs, FPCB NPs, and FPCB/HCPT NPs in LLC and A549 cells. Cell viability of LLC (A) and A549 (B) cells treated with 10 μg/mL of BA, HCPT, and nanoparticles (equivalent to native BA) was measured by CCK-8 assay (n=3, error bars represent standard deviation). CCK-8 assay of BA, HCPT, CMC-PEG, and nanoparticles with different concentrations in LLC (C) and A549 (D) cell lines (n=3, error bars represent standard deviation).

Journal of Materials Chemistry B

Dynamic Article Links ►

Cite this: DOI: 10.1039/c0xx00000x

PAPER

www.rsc.org/xxxxxx

Table 2 *In vitro* Cytotoxicity Analysis (IC_{50}, μg/mL)

Compound	LLC	A549
BA	6.35 (0.51935)	8.54 (0.52357)
HCPT	0.31 (0.02936)	0.46 (0.03682)
PCB NPs	3.89 (0.22748)	6.53 (0.48632)
FPCB NPs	2.80 (0.21244)	5.92 (0.39276)
FPCB/HCPT NPs	0.07 (0.00235)	0.23 (0.00261)

To compare the potency of the medicine, the concentration of drug it takes to kill 50% of the cells (IC_{50}) was estimated from survival curves, including the curves in Fig. 8C and D, obtained from replicate experiments. The results showed that the IC_{50} of the sample is in the order BA > PCB NPs > FPCB NPs > HCPT > FPCB/HCPT NPs (Table 2). Compared to the free BA, the FPCB NPs treatment was 2.3× more toxic against LLC, 1.4× more toxic against A549 and the FPCB/HCPT NPs treatment was 90.7× more toxic against LLC and 37.1× more toxic against A549. Compared to the free HCPT, the FPCB/HCPT NPs treatment was 4.4× more toxic against LLC and 2.0× more toxic against A549. PCB and FPCB are members of a class of conjugates that are more effective than free drug *in vitro*,[52] which might be influenced by polymeric architectures of CMC in conjugation with BA. Moreover, increased FPCB/HCPT NPs toxicity was approximately related to the chemosensitivity of each cell line and slow release of the drugs. In addition to the benefits of slow release, internalization of the polymers and enhanced release in lysosomes may further enhance the action of drugs. Moreover, the combination therapy with BA and HCPT can induce superior *in vitro* therapeutic efficacy versus free drugs. The FPCB/HCPT NPs (22.88 wt% BA, 21.15 wt% HCPT) IC_{50} of LLC and A549 were 0.07 μg/mL and 0.23 μg/mL, the calculated combination index (CI) of BA and HCPT in the FPCB/HCPT NPs were 0.07 (LLC) and 0.17 (A549), which were far smaller than 1. This suggested that FPCB/HCPT NPs achieve the significant synergistic effect by co-delivery two different anticancer drugs BA and HCPT.[38]

3.6. Folate Competition

In order to further evaluate the role of folate in the cellular uptake of FPCB/HCPT NPs, LLC cells and A549 cells were employed as folate receptor (FR) overexpressing cancer cells and FR deficiency cancer cells, respectively.[53, 54] The cells were incubated with the nanoparticles (0.1 μg/mL) in culture medium containing increasing concentrations of free folate as described previously with minor modification.[55] The cytotoxicity of FPCB/HCPT NPs against LLC cells was inhibited by excess free folate, and the cell viability increased with increasing folate concentration (Fig. 9A). However, their cytotoxicity against A549 cells did not change as a function of folate concentration (Fig. 9B). For instance, the cell viability of FPCB/HCPT NPs against LLC cells was approximately 15.2% at FPCB/HCPT NPs and free folate concentrations of 0.01 μg/mL, but it was about 40%

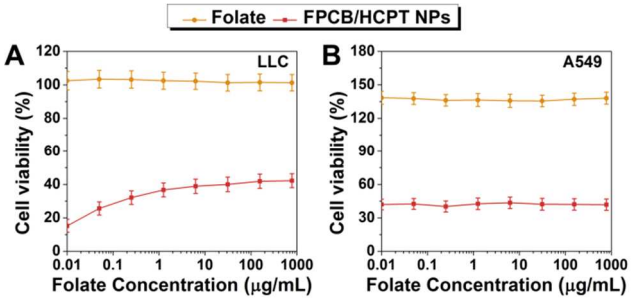

Fig. 9 Effect of free folate on viability of LLC (A) and A549 cells (B) incubated with FPCB/HCPT NPs.

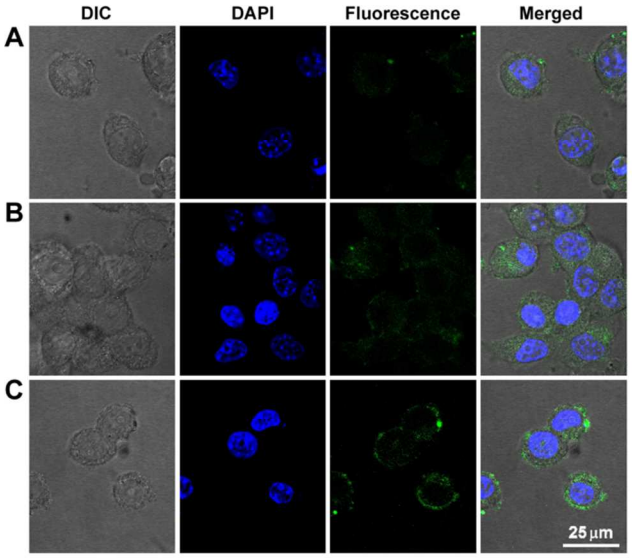

Fig. 10 Confocal microscopic pictures of LLC cells incubated with (A) free HCPT, (B) PCB/HCPT NPs, and (C) FPCB/HCPT NPs at an equivalent HCPT concentration of 0.3 μg/mL (IC_{50}) for 4 h at 37 °C.

in the presence of 30 μg/mL free folate. These findings suggest that free folate molecules prevent the cellular uptake of the nanoparticles by competitive binding to FR on the cell surface.

3.7. Cellular Uptake

As shown in Fig. 10, the cellular uptake efficiencies of HCPT, PCB/HCPT NPs, and FPCB/HCPT NPs were evaluated by CLSM. It can be visualized the fluorescence of HCPT (green) and the DAPI (blue). Free HCPT molecules transported into the cytoplasm of the cell, in a passive diffusion manner, were effluxed out by P-glycoprotein pumps, while some of them could reach into the nucleus and bind to DNA. In general, HCPT-loaded nano-particulates, such as liposomes, micelles, polymer nanoparticles, have been known to be taken up by cells through an endocytic pathway, thereby making them escape from the

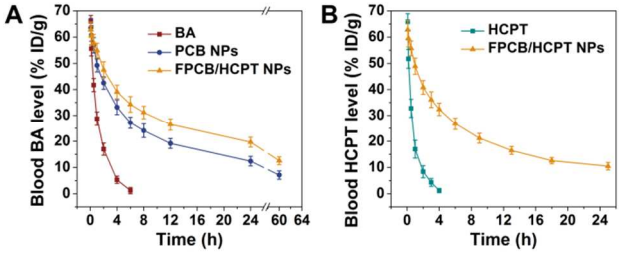

Fig. 11 Blood circulation curves and half-time of PCB NPs, FPCB/HCPT NPs compared with free BA (A), and FPCB/HCPT NPs compared with free HCPT. Error bars were based on six mice per group at each time point.

effect of P-glycoprotein pumps.[56] The endocytic delivery of HCPT within cells by using nanoparticles maintains the intracellular HCPT concentration to be high in the cytoplasm region. This can be seen in Fig. 10A and B. Cellular uptake extent of FPCB/HCPT NPs was significantly higher than those of free HCPT and PCB/HCPT NPs under the same condition. In Fig. 10C, it is of interest to note that FPCB/HCPT NPs are densely located around the cytoplasm region near the cell membrane. It can be visualized that FPCB/HCPT NPs were primarily located on the surface of cell membrane, due to their preferential binding to folate receptors on the membrane.[25]

3.8. The Pharmacokinetics in Mice

Long blood circulation half-time of a drug carrier is desired to improve the bioavailability of the drug. The determined drug concentration after hydrolysis under basic condition was actually the total BA or HCPT in plasma, the combination of both parent form and nanoparticles form. The plasma clearance curves of free BA, HCPT, and nanoparticles in mice were shown in Fig. 11A and B. Disappearance of free BA and free HCPT from the blood circulation after intravenous administration of injection was very rapid with the plasma concentration below 10% of injected dose per gram (% ID/g) at 3 h and 2 h, respectively. On the contrary, PCB NPs and FPCB/HCPT NPs exhibited a remarkable prolonged clearance with the BA levels of 12.4% and 19.7% ID/g at 24 h after administration. For HCPT levels, FPCB/HCPT NPs exhibited 10.5% ID/g at 25 h after administration. The blood circulation half-time of free BA were 0.8 h. PCB NPs, and FPCB/HCPT NPs could extend the blood circulation half-time of BA from 0.8 h to 3.6 h and 5.1 h, respectively, which were far longer (4.5- and 6.4-fold compared with free BA) than values of BA. FPCB/HCPT NPs could extend the blood circulation half-time of HCPT from 0.5 h to 3.0 h.

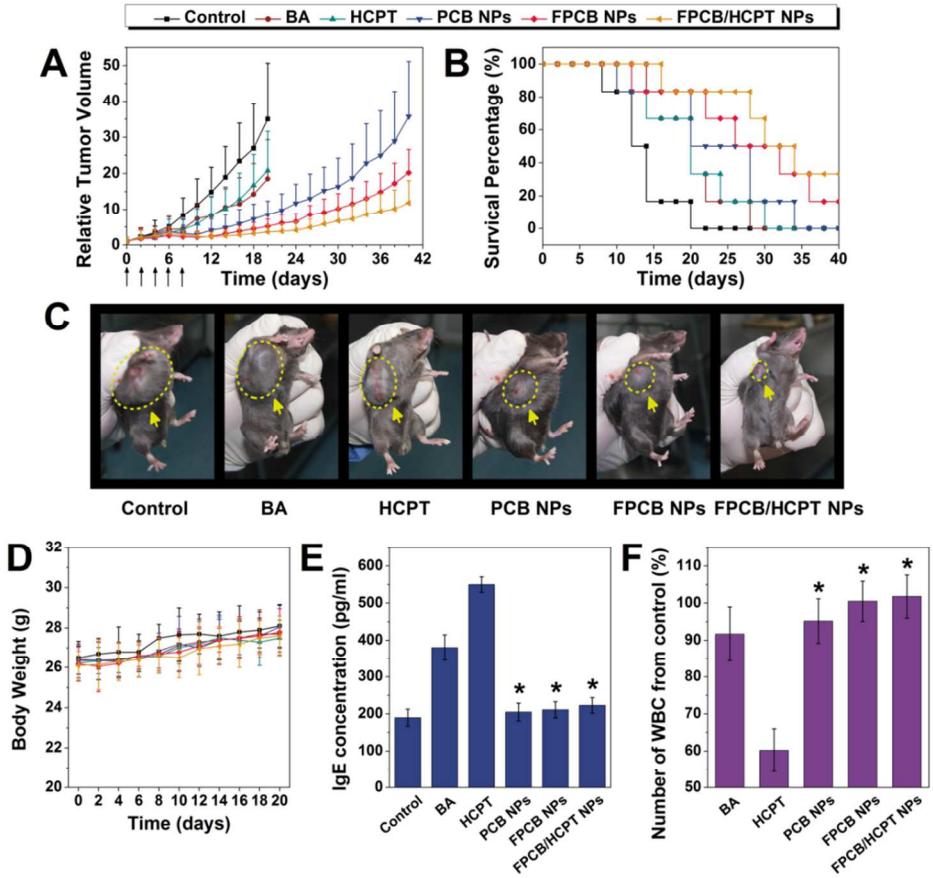

Fig. 12 *In vivo* antitumor activity of free BA, free HCPT, and nanoparticles in the subcutaneous mouse model of LLC. (A) Tumor volumes of mice during treatment with different groups. (B) Survival of mice in different treatment. (C) Tumor photographs from each treatment group excised on day 20. (D) The animal weights were recorded once per week and expressed over the 20 day observation. (E) White blood cell (WBC) change during four administrations in normal mice with free BA, free HCPT, and nanoparticles. Blood sample was collected from mice on day 2 after the last dosage treatment. (F) IgE levels of mice treated with free BA, free HCPT, and nanoparticles for 30 min. Data as means ± SD; n = 6.

Journal of Materials Chemistry B

Cite this: DOI: 10.1039/c0xx00000x

www.rsc.org/xxxxxx

PAPER

Table 3 LLC Xenograft Model (q2d × 5): Efficacy Comparison

Compound	mean TV±SD (mm^3)[a]	RTV[a]	TGI(%)[a]	Cures(%)[b]
control	4530 ± 2019	35.0 ± 15.6	0	0
BA	2387 ± 1393	18.5 ± 10.8	47.3	16.7
HCPT	2787 ± 1500	20.8 ± 11.2	38.5	16.7
PCB NPs	935 ± 418	8.5 ± 3.8	79.3	50.0
FPCB NPs	650 ± 250	5.2 ± 2.0	85.6	66.7
FPCB/HCPT NPs	439 ± 183	3.6 ± 1.5	90.3	83.3

[a] Mean tumor volume (TV), RTV, and % TGI data were taken at day 20. (By day 20, a significant percentage of control animals were euthanized due to excess tumor burden.) [b] % cures were taken at day 26.

3.9. *In vivo* Studies

The results described above gave us great confidence to evaluate the anticancer effectiveness of BA formulations in a mouse tumor model. The efficacies of drug delivery nanoparticles were compared with free BA and HCPT at equivalent doses of 10 mg/kg BA and 10 mg/kg HCPT, respectively, on multiple-dose schedule in xenograft models of lung tumor. For humane reasons, animals were killed and regarded as dead if the implanted tumor volume reached 5000 mm^3 or at the end of the experiment (> 6 weeks). The two most important goals in cancer treatment are prolonged survival without reduction in the quality of life. Tumor-bearing mice treated with the nanoparticles showed a clear survival advantage compared with the control treated mice (Fig. 12B). As shown in Fig. 12A, the groups treated with BA, HCPT, and different nanoparticles showed varied levels of antitumor effects and they were ranked as FPCB/HCPT NPs > FPCB NPs > PCB NPs > BA and HCPT. The treatment with FPCB/HCPT NPs resulted in 90.3% TGI (day 20) and 83.3% survival of animals (day 26). In contrast, multiple-dose free BA treatment resulted in 47.3% TGI (day 20), 16.7% survival of animals (day 26), and free HCPT treatment resulted in 38.5% TGI (day 20) and 16.7% survival of animals (day 26) (Table 3, Fig. 12A and B). Importantly, in line with the literature, no signs of systemic toxicity were observed by monitoring general behavior, appetite and mice body weight (Fig. 12D).

As expected, when using the HCPT-encapsulated FPCB NPs for *in vivo* anticancer therapy, two effects are anticipated to increase the anticancer efficacy of the drug-loaded nanoparticles: (1) the appropriate size (~180 nm), the EPR effect of solid tumors would allow more drug-loaded nanoparticles to be accumulated in the tumor tissue;[15] (2) high drug loading and synergetic effect (~ 23 wt% BA and ~ 21 wt% HCPT); (3) drug-loaded nanoparticles can increase the solubility of the drug.[57] In addition, the *in vitro* and *in vivo* experiments (Fig. 8 and 12) demonstrate that the FPCB NPs has better therapeutic efficacy than PCB NPs, which may due to the active targeting effect of folic acid.

3.10. Evaluation of the Side Effects

Although the drug delivery nanoparticles showed significant therapeutic effects *in vivo*, whether these nanoparticles had non-negligible adverse effects remained a critical issue. During its early development, type I hypersensitivity is the most common type of the hypersensitivity reaction. Some of the natural anticancer drugs, such as paclitaxel, docetaxel, and teniposide cyclosporine, were usually associated with a high incidence of the type I hypersensitivity reaction. It has been demonstrated that IgE antibodies play an important part in mediating type I hypersensitivity responses. We thus selected IgE levels as the parameter for rapid evaluation of type I hypersensitivity reactions. The blood IgE levels of mice in different groups (BA, HCPT, PCB NPs, FPCB NPs, and FPCB/HCPT NPs) were shown in Fig. 12E. Mice treated with BA and HCPT displayed a higher IgE level than the control group, which might be ascribed to the bad water solubility. As expected, no significant change of IgE level was observed in the PCB NPs, FPCB NPs, and FPCB/HCPT NPs groups, which explored the idea that the use of these nanoparticles could reduce the risk of hypersensitivity reactions substantially. The blood of mice after treatment with different formulations was also collected to test the WBC count, which is often used as an indicator of hematologic toxicity. The total WBC count of mice treated with BA and HCPT showed a decrease over the normal group (Fig. 12F). No discernible decreases in WBC number of the mice treated with the PCB NPs, FPCB NPs, and FPCB/HCPT NPs groups were observed, indicating that the nanoparticles designed in this study could avoid severe hematotoxicity.

4. Conclusion

By the necessary chemical functionalization of cellulose, we had developed an amphiphilic targeted nanoparticle platform consisting of a hydrophobic anticancer core of BA and a hydrophilic shell of CMC and PEG (PEG-folate), which is capable of entrapping another anticancer drug HCPT to develop a FPCB/HCPT targeted nanoparticulate delivery system. The therapeutic efficacy of the FPCB/HCPT NPs was better than those of free BA, HCPT, PCB NPs, and FPCB NPs. This nanoparticle for co-delivery of anticancer drugs demonstrated a series of attractive properties as an anticancer drug delivery carrier, including ease of preparation, appropriate size, high loading capacity of drugs, good stability, rapid cellular uptake by tumor cells, high synergistic effects, and few side effects.

Acknowledgements

This study was funded by the Fundamental Research Funds for the Central Universities (200-1244951), the State Forestry Administration 948 Project of China (No. 2014-4-35), Beijing Natural Science Foundation of China (Grant No. 2142024), the National High Technology Research and Development Program of China (863 Program, No. 2014AA022109), and the National Natural Science Foundation of China (No. 20976179).

Notes and references

[a] *Beijing Key Laboratory of Lignocellulosic Chemistry, Beijing Forestry University, Beijing 100083, P. R. China. Fax/Tel: 8610-62338152; E-mail: ljd2012@bjfu.edu.cn (J.D. Lei)*
[b] *Tianjin Key Laboratory of Pulp & Paper, College of Materials Science & Chemical Engineering, Tianjin University of Science & Technology, Tianjin 300457, P. R. China*
[c] *Yuannan Pharmaceutical Industrial Co., Ltd, Kunming 650106, P. R. China. E-mail: 892660242@qq.com (G.Q. Guo)*

1. E. Pisha, H. Chai, I.-S. Lee, T. E. Chagwedera, N. R. Farnsworth, G. A. Cordell, C. W. W. Beecher, H. H. S. Fong, A. D. Kinghorn, D. M. Brown, M. C. Wani, M. E. Wall, T. J. Hieken, T. K. Das Gupta and J. M. Pezzuto, *Nat Med*, 1995, **1**, 1046-1051.
2. M. E. Wall, M. C. Wani, C. E. Cook, K. H. Palmer, A. T. McPhail and G. A. Sim, *Journal of the American Chemical Society*, 1966, **88**, 3888-3890.
3. R. V. Smalley, J. Carpenter, A. Bartolucci, C. Vogel and S. Krauss, *Cancer*, 1977, **40**, 625-632.
4. M. Harries and M. Gore, *The Lancet Oncology*, 2002, **3**, 529-536.
5. A. Saleem, T. K. Edwards, Z. Rasheed and E. H. Rubin, *Annals of the New York Academy of Sciences*, 2000, **922**, 46-55.
6. Y. Sugimoto, S. Tsukahara, T. Oh-hara, L. F. Liu and T. Tsuruo, *Cancer Research*, 1990, **50**, 7962-7965.
7. H.-J. Jeong, H.-B. Chai, S.-Y. Park and D. S. H. L. Kim, *Bioorganic & medicinal chemistry letters*, 1999, **9**, 1201-1204.
8. F. Danhier, O. Feron and V. Preat, *Journal of controlled release : official journal of the Controlled Release Society*, 2010, **148**, 135-146.
9. V. P. Torchilin, *Pharmaceutical research*, 2007, **24**, 1-16.
10. Y. Mi, Y. Liu and S. S. Feng, *Biomaterials*, 2011, **32**, 4058-4066.
11. K. Kim, S. Kwon, J. H. Park, H. Chung, S. Y. Jeong, I. C. Kwon and I. S. Kim, *Biomacromolecules*, 2005, **6**, 1154-1158.
12. J. H. Kim, Y. S. Kim, S. Kim, J. H. Park, K. Kim, K. Choi, H. Chung, S. Y. Jeong, R. W. Park, I. S. Kim and I. C. Kwon, *Journal of controlled release : official journal of the Controlled Release Society*, 2006, **111**, 228-234.
13. H. Maeda, J. Wu, T. Sawa, Y. Matsumura and K. Hori, *Journal of Controlled Release*, 2000, **65**, 271-284.
14. H. Maeda, *Bioconjugate chemistry*, 2010, **21**, 797-802.
15. H. Maeda, *Journal of Controlled Release*, 2012, **164**, 138-144.
16. A. S. Turaev, *Chem Nat Compd*, 1995, **31**, 254-259.
17. J. Xu, S. Strandman, J. X. X. Zhu, J. Barralet and M. Cerruti, *Biomaterials*, 2015, **37**, 395-404.
18. Y. Yang, S. Wang, Y. Wang, X. Wang, Q. Wang and M. Chen, *Biotechnology Advances*, 2014, **32**, 1301-1316.
19. K.-J. Chen, H.-F. Liang, H.-L. Chen, Y. Wang, P.-Y. Cheng, H.-L. Liu, Y. Xia and H.-W. Sung, *ACS Nano*, 2013, **7**, 438-446.
20. E. Auzenne, S. C. Ghosh, M. Khodadadian, B. Rivera, D. Farquhar, R. E. Price, M. Ravoori, V. Kundra, R. S. Freedman and J. Klostergaard, *Neoplasia*, 2007, **9**, 479-486.
21. M. J. Ernsting, W. L. Tang, N. MacCallum and S. D. Li, *Bioconjugate chemistry*, 2011, **22**, 2474-2486.
22. S. D. Weitman, A. G. Weinberg, L. R. Coney, V. R. Zurawski, D. S. Jennings and B. A. Kamen, *Cancer Research*, 1992, **52**, 6708-6711.
23. Y. Iwasaki, H. Maie and K. Akiyoshi, *Biomacromolecules*, 2007, **8**, 3162-3168.
24. W. Xia and P. S. Low, *Journal of Medicinal Chemistry*, 2010, **53**, 6811-6824.
25. P. S. Low and S. A. Kularatne, *Current Opinion in Chemical Biology*, 2009, **13**, 256-262.
26. Y. Lu and P. S. Low, *Advanced Drug Delivery Reviews*, 2012, **64, Supplement**, 342-352.
27. C. M. Paulos, M. J. Turk, G. J. Breur and P. S. Low, *Advanced Drug Delivery Reviews*, 2004, **56**, 1205-1217.
28. D. Kim, E. Lee, K. Park, I. Kwon and Y. Bae, *Pharmaceutical research*, 2008, **25**, 2074-2082.
29. L. Brannon-Peppas and J. O. Blanchette, *Advanced Drug Delivery Reviews*, 2012, **64, Supplement**, 206-212.
30. N. Parker, M. J. Turk, E. Westrick, J. D. Lewis, P. S. Low and C. P. Leamon, *Analytical Biochemistry*, 2005, **338**, 284-293.
31. Y. Wang, Y. Wang, J. Xiang and K. Yao, *Biomacromolecules*, 2010, **11**, 3531-3538.
32. S. Wang, R. J. Lee, C. J. Mathias, M. A. Green and P. S. Low, *Bioconjugate chemistry*, 1996, **7**, 56-62.
33. C. J. Mathias, S. Wang, P. S. Low, D. J. Waters and M. A. Green, *Nuclear medicine and biology*, 1999, **26**, 23-25.
34. H.-Y. Cheung and Q.-F. Zhang, *Journal of Chromatography A*, 2008, **1213**, 231-238.
35. J. Nguyen, T. W. J. Steele, O. Merkel, R. Reul and T. Kissel, *Journal of Controlled Release*, 2008, **132**, 243-251.
36. R. Reul, J. Nguyen and T. Kissel, *Biomaterials*, 2009, **30**, 5815-5824.
37. F. Unger, M. Wittmar and T. Kissel, *Biomaterials*, 2007, **28**, 1610-1619.
38. T.-C. Chou, *Cancer Research*, 2010, **70**, 440-446.
39. B. Shi, C. Fang and Y. Pei, *Journal of pharmaceutical sciences*, 2006, **95**, 1873-1887.
40. W. C. Huang, W. H. Chiang, Y. F. Huang, S. C. Lin, Z. F. Shih, C. S. Chern, C. S. Chiang and H. C. Chiu, *J Drug Target*, 2011, **19**, 944-953.
41. M. J. Ernsting, M. Murakami, E. Undzys, A. Aman, B. Press and S. D. Li, *Journal of controlled release : official journal of the Controlled Release Society*, 2012, **162**, 575-581.
42. C. Peng, G. Bodenhausen, S. Qiu, H. H. S. Fong, N. R. Farnsworth, S. Yuan and C. Zheng, *Magnetic Resonance in Chemistry*, 1998, **36**, 267-278.
43. H. Zhao, B. Rubio, P. Sapra, D. C. Wu, P. Reddy, P. Sai, A. Martinez, Y. Gao, Y. Lozanguiez, C. Longley, L. M. Greenberger and I. D. Horak, *Bioconjugate chemistry*, 2008, **19**, 849-859.
44. L. Zhang, F. X. Gu, J. M. Chan, A. Z. Wang, R. S. Langer and O. C. Farokhzad, *Clinical Pharmacology & Therapeutics*, 2008, **83**, 761-769.
45. U. Bilati, E. Allémann and E. Doelker, *European Journal of Pharmaceutical Sciences*, 2005, **24**, 67-75.
46. Y. Sanada, I. Akiba, K. Sakurai, K. Shiraishi, M. Yokoyama, E. Mylonas, N. Ohta, N. Yagi, Y. Shinohara and Y. Amemiya, *Journal of the American Chemical Society*, 2013, **135**, 2574-2582.
47. Y. Shen, E. Jin, B. Zhang, C. J. Murphy, M. Sui, J. Zhao, J. Wang, J. Tang, M. Fan, E. Van Kirk and W. J. Murdoch, *Journal of the American Chemical Society*, 2010, **132**, 4259-4265.
48. M. Gao, P. M. Lau and S. K. Kong, *Archives of toxicology*, 2014, **88**, 755-768.
49. Y. Zhang, S. F. Ali, E. Dervishi, Y. Xu, Z. Li, D. Casciano and A. S. Biris, *ACS Nano*, 2010, **4**, 3181-3186.
50. C. Ge, J. Du, L. Zhao, L. Wang, Y. Liu, D. Li, Y. Yang, R. Zhou, Y. Zhao, Z. Chai and C. Chen, *Proceedings of the National Academy of Sciences*, 2011, **108**, 16968-16973.
51. T. Lammers, W. E. Hennink and G. Storm, *Br J Cancer*, 2008, **99**, 392-397.

52. J. J. Khandare, S. Jayant, A. Singh, P. Chandna, Y. Wang, N. Vorsa and T. Minko, *Bioconjugate chemistry*, 2006, **17**, 1464-1472.
53. S. B. Gates, L. G. Mendelsohn, K. A. Shackelford, L. L. Habeck, J. D. Kursar, L. S. Gossett, J. F. Worzalla, C. Shih and G. B. Grindey, *Clinical Cancer Research*, 1996, **2**, 1135-1141.
54. D. J. Bharali, D. W. Lucey, H. Jayakumar, H. E. Pudavar and P. N. Prasad, *Journal of the American Chemical Society*, 2005, **127**, 11364-11371.
55. K. S. Soppimath, L. H. Liu, W. Y. Seow, S. Q. Liu, R. Powell, P. Chan and Y. Y. Yang, *Advanced Functional Materials*, 2007, **17**, 355-362.
56. A. A. Gabizon, *Cancer Research*, 1992, **52**, 891-896.
57. O. P. Medina, N. Pillarsetty, A. Glekas, B. Punzalan, V. Longo, M. Gönen, P. Zanzonico, P. Smith-Jones and S. M. Larson, *Journal of Controlled Release*, 2011, **149**, 292-298.

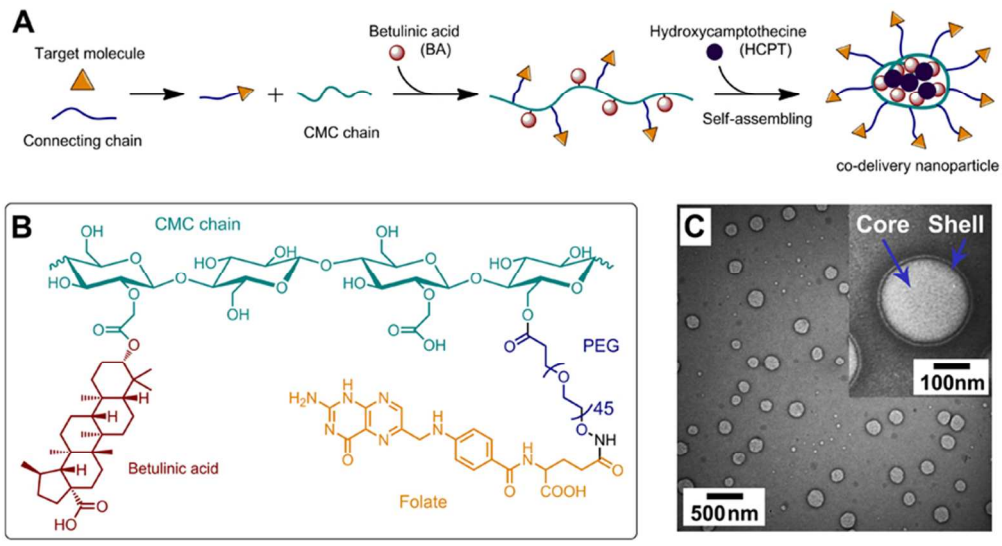

The folate-PEG-carboxymethylcellulose-betulinic acid was synthesized by introducing folate, PEG, betulinic acid to carboxymethylcellulose, then self-assembled into nanoparticle with HCPT encapsulated.
74x39mm (300 x 300 DPI)